Journal of Materials Chemistry B

Accepted Manuscript

ROYAL SOCIETY OF CHEMISTRY

www.rsc.org/materialsB

Cite this: DOI: 10.1039/c0xx00000x

www.rsc.org/xxxxxx

ARTICLE TYPE

Hydroxyapatite Coatings with Oriented Nanoplate Arrays: Synthesis, Formation Mechanism and Cytocompatibility

Jun-Jie Guan,†[a,c] Bo Tian,†[b] Sha Tang,[a] Qin-Fei Ke,[a] Chang-Qing Zhang,[c] Zhen-An Zhu,*[b] and Ya-Ping Guo*[a]

Received (in XXX, XXX) Xth XXXXXXXXX 20XX, Accepted Xth XXXXXXXXX 20XX
DOI: 10.1039/b000000x6

Hydroxyapatite (HA) is the main inorganic constituent of natural bones and teeth with the *c*-axis orientation and *a*(*b*)-axis orientation, respectively. Designing of HA coatings (HACs) with specific orientation and morphology is an important strategy to improve their biological properties. Herein, we report, for the first time, the hydrothermal synthesis of HACs with oriented nanoplate arrays according to the following steps: (i) deposition of brushite/chitosan coatings (BCCs) on Ti6Al4V substrates; and (ii) transformation of HACs with oriented nanoplate arrays from BCCs after hydrothermal treatment with alkaline solutions. After soaking the BCCs in a NaOH solution under hydrothermal conditions, the Ca^{2+} and PO_4^{3-} ions are released from the coatings because of the dissolution reaction of brushite, and react with OH^- ions to form HA nanoplates. Interestingly, these HA nanoplates with a preferential *c*-plane orientation are perpendicular to the coating surfaces. Hydrothermal reaction time and Ca/P ratio of BCCs have great effect on the morphologies of HA nanoplates. With increasing the reaction time from 3 h to 3 days or decreasing the Ca/P ratio from 2.0 to1.0, the widths (or lengths) of HA nanoplates increase gradually. Simulated body fluid immersion (SBF) tests reveal that the HACs with oriented nanoplate arrays can promote the formation of apatite on the surfaces, suggesting their good *in vitro* bioactivity. Moreover, human bone marrow stromal cells (hBMSCs) have been used as cell models to investigate cytocompatibility of the HACs. The hBMSCs on the HACs have better cell adhesion, spreading, proliferation and osteogenic differentiation than on Ti6Al4V substrates because the HACs are similar to the minerals of human hard tissues in chemical composition, morphology and crystallographic orientation. Therefore, HACs with oriented nanoplate arrays have great potentials for implants of human hard tissues.

1. Introduction

Reconstructions of skeletal defects arising from osteoporosis, tumour resection and bone trauma are still complicated challenges in the field of orthopaedic surgery.[1] Titanium alloys have been widely used for bone implants under load-bearing conditions because of their low density, good corrosion resistance and excellent mechanical properties.[2] However, their bio-inert property limits their clinical applications. Recently, biocoatings on medical metal substrates have developed because they combine the mechanical advantages of titanium alloys with the excellent biological properties of bioactive materials.[3] Notably, the bioactivity, osseointegration and biocompatibility of biocoatings depend mainly on chemical composition, crystallographic texture and morphology.

Carbonated calcium-deficient apatite is the major inorganic constituent of natural bones, and the corresponding synthetic hydroxyapatite ($Ca_{10}(PO_4)_6(OH)_2$, HA) has been widely used for bone implant, bone filling material and teeth root.[4] In vertebrate bones and tooth enamel surfaces, HA crystals exhibit *c*-axis orientation and *a*(*b*)-axis orientation, respectively. Previous researchers have demonstrated that highly *c*-axis oriented HA coatings (HACs) have higher hardness and Young's modulus values than randomly oriented HACs.[5] Moreover, well aligned, ordered HA structures can promote initial adhesion, long-term growth, differentiation of MG-63 osteoblast-like cells, and accelerate mineralized tissue formation.[5]

Hexagonal HA crystals with a $P6_3/m$ space group have two crystal planes including *a*(*b*)-plane (*ac* and *bc* crystal faces) and *c*-plane (*ab* crystal face).[6] The *a*(*b*)-plane of HA crystals are rich in calcium ions, while the *c*-planes are rich in phosphate and hydroxide ions.[6] HA crystals with different crystallographic orientations exhibit different biological properties including biocompatibility, bioactivity and biodegradability. Up to now, several coating methods such as electrochemical deposition, ZnO-seeded method and hydrothermal method have been developed to fabricate HACs with oriented nanorod arrays composed of nano/micro HA single crystals.[7] The HA crystals on the above coatings exhibit a rod-like structure with a *c*-axis orientation. It is noted that HA nanocrystals in natural bones exist as plate-like shapes with thicknesses of 2-7 nm, lengths and widths of 30-200 nm.[8] Although plate-like HACs have been

fabricated in recent years, the HA plates exhibit only weak a(b)-axis orientations and are polycrystalline.[9] The synthesis of HACs with oriented nanoplate arrays still remains great challenge.

The biomineralization mechanism of natural bones provide an important way to design and fabricate ideal bone implants.[8] During biomineralization of bone minerals, apatite nanocrystals are converted from amorphous calcium phosphate by using metastable crystalline phases such as octacalcium phosphate (OCP, $Ca_8H_2(PO_4)_6·5H_2O$) and brushite (DCPD, $CaHPO_4·2H_2O$) as transitory precursors.[8] Herein, we mimicked the formation process of HA in natural bone to fabricate HACs with oriented nanoplate arrays by using DCPD/chitosan coatings (BCCs) as precursors. The preparation process included the following stages: (i) preparation of precursor solutions including Ca^{2+} ions, PO_4^{3-} ions and chitosan, (ii) deposition of BCCs on Ti6Al4V substrates by dip-coating method; and (iii) transformation of HACs with oriented nanoplate arrays from BCCs after hydrothermal treatment with alkaline solutions. The main aims of this work were to fabricate HACs with oriented nanoplate arrays, and to study their structure, morphology, formation mechanism, cytocompatibility and osteoinductivity.

2. Experimental

2.1 Materials

Titanium alloys (Ti6Al4V) substrates were purchased from Baoji Tiint Medical Ti CO., Ltd. Hydrochloric acid, phosphoric acid, hydrofluoric acid, acetic acid, sodium dihydrogen phosphate, calcium nitrate, sodium hydroxide, sodium chloride, sodium hydrogen carbonate, potassium chloride, dipotassium hydrogen phosphate, magnesium chloride, calcium chloride and sodium sulfate were purchased from National Medicine Group Chemical Reagent Co., Ltd. Chitosan (85% deacetylated form), trihydroxymethyl aminomethane, 4′,6 diamidino-2-phenylindole (DAPI), dexamethasone, tetramethylrhodamine isothiocyanate (TRITC) phalloidin, ascorbate acid, paraformaldehyde, β-glycerophosphate sodium (β-GP), alizarin red solution, cetylpyridinum chloride, cetylpyridinum chloride and sodium phosphate were obtained from Sigma Aldrich, USA. Alpha modification of Eagles medium (a-MEM), fetal bovine serum (FBS) and *p*-nitrophenyl phosphate (pNPP) were purchased from Gibco-BRL, Sydney, Australia. Penicillin and streptomycin were purchased from Hyclone, USA. CCK-8 was obtained from Dojindo Molecular Technology, Japan. All chemicals used in this study were of analytical grade.

2.2 Preparation of HACs

Titanium alloys (Ti6Al4V), $15\times15\times0.9$ mm^3 in size, were used for substrate materials. Before deposition, the substrates were abraded with 1000-grit SiC paper and washed with pure acetone and deionized water in an ultrasonic cleaner. Acid treatment was performed by soaking these substrates in a 1.0 mol/L H_3PO_4-1.5 wt% HF solution for 20 min at room temperature, to form a layer of TiO_x gel on their surfaces. After the acid treatment, the substrates were gently washed with deionized water, and dried at room temperature in an air atmosphere.

The biomedical grade chitosan (3.4×10^5 g/mol of viscosity-average molecular weight and 91% of deacetylation degree) was supplied by Qingdao Haihui Bioengineering Co., Ltd. 1.000 g of chitosan powders were dissolved to 100 ml of an acetic acid solution (2.0 vt%) under vigorous agitation to obtain a homogeneous chitosan/acetic acid solution. $Ca(NO_3)_2·4H_2O$ (2.362 g) and $NaH_2PO_4·2H_2O$ (0.780 g, 0.936 g or 1.560 g) were added into the chitosan/acetic acid solution at room temperature. The corresponding Ca/P molar ratios in the solutions were 2.0, 1.67 and 1.0, respectively. The Ti6Al4V substrates were dipped in the above solutions for 5 s, and then were withdrawn in a rate of 1 mm/s. The as-obtained coatings were abbreviated as CCPs. After drying the CCPs at room temperature for 48 h, BCCs including DCPD/chitosan coatings were prepared. The BCCs were immersed in a NaOH solution (5 wt%) in Teflon-lined stainless steel autoclave, and hydrothermally reacted at 120°C for 2 h, 24 h and 3 days, respectively. Finally, the products (HACs) were washed with deionized water, and then dried at 60°C for 48 h.

2.2 Characterization

The morphology and microstructure of samples were investigated by using scanning electron microscopy (SEM, Hitachi S-4800, CamScan) with energy-dispersive spectrometry (EDS) and transmission electron microscopy (TEM, CM200/FEG, Philips) with electron diffraction (ED). Fourier transform infrared (FTIR, VECTOR22, BRUKER) spectra were collected by using the KBr pellet technique. The phases of samples were examined by X-ray powder diffraction (XRD, D/max-II B, Japan). The thermal behaviors of samples were examined by thermo-gravimetric analysis (TG-DTA, Perkin-Elmer) at a heating rate of 10 °C/min in an alumina crucible in air atmosphere.

2.3 *In vitro* bioactivity of HACs

A simulated body fluid (SBF) with ion concentrations approximately equal to those of human blood plasma has been used widely to investigate the *in vitro* bioactivity of biomateirals.[10] SBF was prepared by dissolving reagent grade chemicals of NaCl, $NaHCO_3$, KCl, $K_2HPO_4·3H_2O$, $MgCl_2·6H_2O$, $CaCl_2$, Na_2SO_4, and $(CH_2OH)_3CNH_2$ into deionized water, and buffering it at pH 7.40 with hydrochloric acid at 37°C. The HACs which were converted from BCCs with a Ca/P ratio of 1.67 by hydrothermal reaction at 120°C for 24 h were soaked in 25 ml of SBF, and kept at 37°C. After given periods of time (6 h, 12 h, 1 day, 2 days, 3 days, 5 days, 7 days), the samples were removed from the SBF, washed with deionized water and dried at room temperature. The concentrations of phosphorus and calcium in SBF were determined by using inductively coupled plasma optical emission spectroscopy (ICP-OES, Optima 5300DV, Perkin-Elmer).

2.4 Proliferation and morphology of hBMSCs

This study was approved by the Ethic Committee of the Ninth People's Hospital of Shanghai Jiao Tong University. Human bone mesenchymal stem cells (hBMSCs) were isolated and expanded by using the standard method as described previously.[11] The donor was healthy without metabolic disease, inherited illnesses or other diseases. The hBMSCs were grown in complete α-MEM supplemented with 10% FBS and antibiotics (100 U/ml

penicillin and 100 μg/ml streptomycin) in a 37°C humidified atmosphere with 5% CO_2. The cells at a passage from P3 to P4 were used for these experiments. In addition, in order to investigate the cytocompatibility of the HACs, Ti6Al4V substrates were used as the control.

The cytoskeleton of hBMSCs on samples was observed by using double fluorescence staining.[12] Briefly, hBMSCs were seeded on HACs and Ti6Al4V at a density of 3×10^4 cells per sample in a 12-well plate in triplicate, respectively. After incubation for 24h, the samples were gently washed with PBS and maintained in 4 % paraformaldehyde for 15 min, followed by soaking in 0.1 % Triton X solution for 15 min. TRITC phalloidin was used to stain the actin filaments of cells, and 4',6-diamidino-2-phenylindole (DAPI) was used to stain the nucleation of cells. The cell morphology and spreading of hBMSCs were investigated by using confocal laser scanning microscopy (CLSM, Leica TCS SP2; Leica Microsystems, Heidelberg, Germany).

The proliferation of hBMSCs on HACs and Ti6Al4V was examined with a cell counting Kit-8 (CCK-8, Dojindo Molecular Technology, Japan) assay.[12] Briefly, hBMSCs were seeded on coating surfaces at a density of 7×10^3 cells per sample in a 12-well plate in triplicate. At each time point, the medium were removed, and 1 mL medium was added into each well with 100 μL CCK-8 according to the manufacturer's instructions. After incubation for 3 h, optical density (OD) was measured at 450 nm by using an automated plate reader (PerkinElmer).

2.5 Osteogenic differentiation of hBMSCs

For the osteogenesis assay, hBMSCs with a density of 1×10^5 cells/well were used to evaluate the osteogenic differentiation of the HACs and Ti6Al6V substrates. After incubation in a 12-well plate with the substrates for 24 h, the culture medium was changed to osteogenic induction medium. The α-MEM culture medium was supplemented with 10% FBS, 50 μM ascorbate acid, 100 nM dexamethasone and 10 mM β-GP. The medium was renewed every 3 days.

Alkaline phosphatase (ALP) staining was performed according to previous report.[13] The ALP activity of each sample was determined by a colorimetric assay using an ALP reagent with pNPP as the substrate after culturing for 7 and 14 days. The absorbance of as-formed *p*-nitrophenol was measured at 405 nm using a microplate reader (Synergy HT, Bio-Tek). The total protein content was determined using the BCA protein assay kit (Pierce, Thermo, Rockford, IL, U.S.A.). ALP activity was expressed as OD value at 405 nm per milligram of total cellular proteins. All experiments were performed in triplicate.

Alizarin red staining was used to analyze calcium nodule formation (mineralization). Cells were grown on the HACs and Ti6Al4V substrates for 24 days in osteogenic inductive culture medium. The cells on the samples were fixed in 4% paraformaldehyde for 15 min and stained with 1% alizarin red solution (pH = 4.20) for 45 min at room temperature. Next, the samples were washed with deionized water until no further orange colour appeared in deionized water and then dried at 37°C. Finally, images of the stained samples were acquired using a digital scanner (Scanjet 2400, HP, Palo Alto, CA, U.S.A.). For quantitative analysis, the orange staining was dissolved in 10% cetylpyridinum chloride (pH = 7.0) in 10 mM sodium phosphate, and the OD values were measured at 620 nm using a microplate reader (SynergyHT,Bio-Tek). The mean OD obtained from the blank control were subtracted from the OD of the test groups.

2.6 Statistical analysis

Data were presented as the mean ± standard deviation from at least three independent experiments. Statistical analyses were performed using a one-way analysis of Variance (ANOVA) followed by the Student-Newman-Keul's test. $p < 0.05$ was considered significant.

3. Results and discussion

3.1 Structure and morphology of HACs

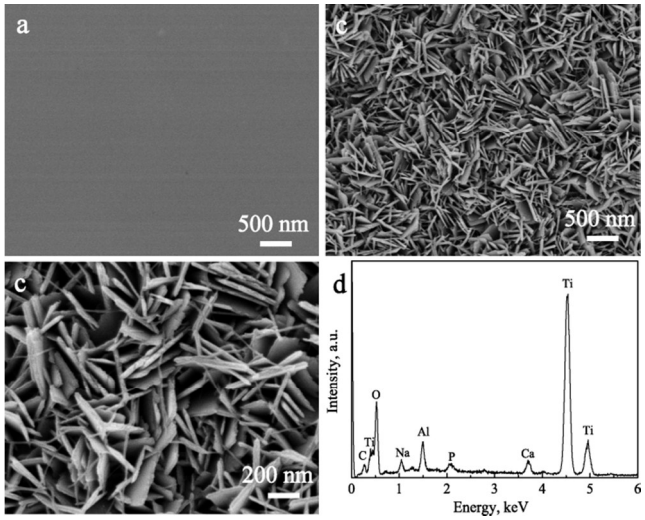

Figure 1 (a) SEM images of BCCs; (b,c) SEM images and (d) EDS spectrum of HACs converted from BCCs with a Ca/P ratio of 1.67 after hydrothermal reaction for 24 h.

During the biomineralization process of natural bones, apatite nanocrystals are converted from amorphous calcium phosphate by using DCPD or OCP as transitory precursors.[8a] In this work, HACs with oriented nanoplate arrays were fabricated according to the following steps. At the first stage, the precursors including chitosan, Ca^{2+} ions and PO_4^{3-} ions were prepared by the addition of $Ca(NO_3)_2\cdot4H_2O$ and $NaH_2PO_4\cdot2H_2O$ into chitosan/acetic acid solutions. At the second stage, the sol-like precursors deposited on Ti6Al4V substrates by dip-coating method. After dried at room temperature for 48 h, DCPD were formed on the coatings (BCCs) due to the volatilization of acetic acid. The SEM image in Figure 1a indicates that the BCCs possess smooth surfaces because the DCPD particles are covered with chitosan. At the final stage, the BCCs were transformed to the HACs with oriented nanoplate arrays after hydrothermal treatment with alkaline solutions at 120°C for 24 h. The low-magnification SEM image in Figure 1b reveals that the HACs are perfectly crack-free coatings. The HA nanoplates with thicknesses of about 10 nm and widths (or lengths) of about 300 nm are perpendicular to the surfaces of the HACs (Figure 1c). Interestingly, the shape of the HA nanoplates is similar to the HA crystals in natural bones, though the particle size of the latter is tinier than the former.[8a] In addition, the HA nanoplates aggregate to produce nonuniform

pores with a pore size of 20-200 nm. The EDS spectrum in Figure 1d reveals that the chemical elements of HACs include Ca, P, O, C, Na, Al and Ti. The Ca, P and O elements are mainly derived from the HA, the Na element might be attributed to the adsorption of Na^+ ions on the coatings or the substitution of the Ca^{2+} ions in HA crystal lattice by Na^+ ions, the C element is derived from chitosan, and the Ti and Al elements are originated from Ti6Al4V substrates.

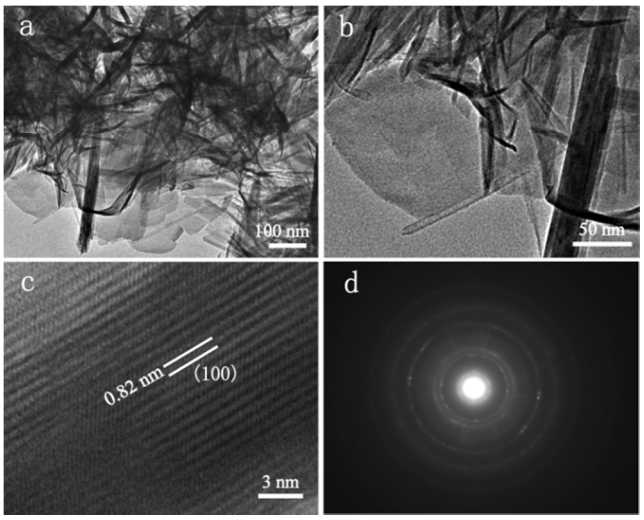

Figure 2 (a,b) Low-resolution TEM images, (c) high-resolution TEM image and (d) corresponding ED pattern of HACs converted from BCCs with a Ca/P ratio of 1.67 after hydrothermal reaction for 24 h.

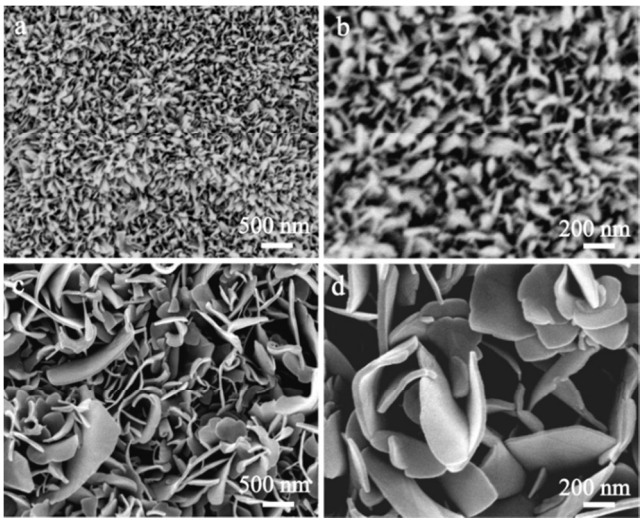

Figure 3 SEM images of HACs converted from CCPs with the Ca/P ratio of 1.67 after hydrothermal reaction for different time: (a,b) 2 h; (c,d) 3 days.

Figure 2 shows the TEM image and ED pattern of the HA nanoplates in the HACs. The low-resolution TEM image confirms that the shape of the HA particles in HACs is plate-like structure, too (Figure 2a and b). The high-resolution TEM image indicates the crystal lattices with a spacing (0.82 nm) that corresponds with the (100) HA planes. Both the SEM images and TEM images suggest that the HA crystals in the HACs possess the *c*-plane orientation (Figures 1 and 2). Moreover, the ED pattern shows the visible diffraction rings, which are indexed to the crystalline HA phase (Figure 2d).

The reaction time has great effects on the morphologies and structures of the HACs. If the reaction time is 2 h, the as-formed HA crystals exhibit plate-like shape (Figures 3a and b). These nanoplates with thicknesses of about 8 nm, widths (or lengths) of about 100 nm are perpendicular to the surfaces of the HACs. With prolonging the reaction time from 2 h to 24 h, the particle size of HA plates grows gradually (Figures 1 and 3). Unfortunately, if the reaction time is prolonged upon 3 days, the obtained HA plates on the HACs exhibit uneven sizes with thicknesses of 50 nm and widths (or lengths) ranging from 100 nm to 800 nm. Moreover, the HA plates begin to curl up (Figures 3c and d).

The effects of reaction time on the structures are investigated by using XRD patterns and FTIR spectra. As we know, calcium phosphate phases mainly include HA, OCP, DCPD and TCP [$Ca_3(PO_4)_2$]. Interestingly, only DCPD exists on the BCCs, as confirmed by the XRD pattern (Figure 4a). After hydrothermal reaction at 120°C for 2 h, the characteristic peaks due to HA crystals are observed in Figure 4b (JCPDS card no. 09-0432). Because of short reaction time, the as-formed HA crystals exhibit a low crystallinity. With prolonging the time from 2 h to 3 days, the characteristic peaks become sharper and stronger, suggesting the increase of HA crystallinity (Figure 4).

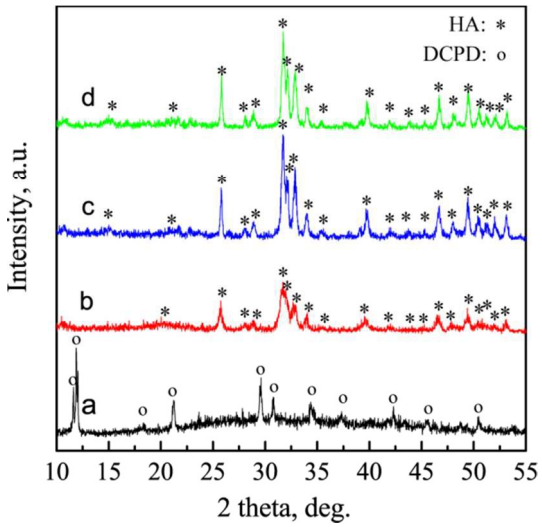

Figure 4 (a) XRD pattern of BCCs with the Ca/P ratio of 1.67; XRD patterns of the HACs converted from the BCCs after hydrothermal reaction at 120°C for different time: (b) 2 h; (c) 1 day; (d) 3 days.

Figure 5a shows the FTIR spectrum of the BCCs before hydrothermal reaction at 120°C for 24 h. The infrared stretching *v*(OH) are observed at 3550, 3489 and 3412 cm^{-1}. The band at 1648 cm^{-1} is ascribed to the H-O-H bending of lattice water molecules.[14] The bands at 1147, 1070, 986 and 877 cm^{-1} are ascribed to P-O stretching vibration in HPO_4^{2-} groups, respectively.[14] The band due to O-P-O(H) bending mode locates at 530 cm^{-1}. The BCCs with the Ca/P ratio of 1.67 are converted to the HACs, after hydrothermal reaction at 120°C for 2h, 24 h and 3 days, respectively. The characterized functional groups of HA crystals are detected for three samples (Figure 5b-d). The intense absorption peak at 1030 cm^{-1} is ascribed to the stretching

vibration (v_3) of the phosphate (PO_4^{3-}) groups, and the absorption peaks at 563 and 604 cm^{-1} are ascribed to the bending vibration (v_4) of the phosphate (PO_4^{3-}) groups.[15] The absorption band due to HPO_4^{2-} at around 1102 cm^{-1} indicates that the samples are calcium deficient HA.[16] The band at 3437 cm^{-1} is corresponding to adsorbed water on the HACs.[17] The hydroxyl absorption bands due to HA are detected at 636 and 3703 cm^{-1}.[18] The weak bands at around 3571 cm^{-1} are ascribed to OH group with weak interactions to the environment.[17] The above results of SEM images, XRD patterns and FTIR spectra suggest that the particle sizes and crystallinities of HA crystals on the HACs increase with prolonging reaction time, but the functional groups do not change obviously.

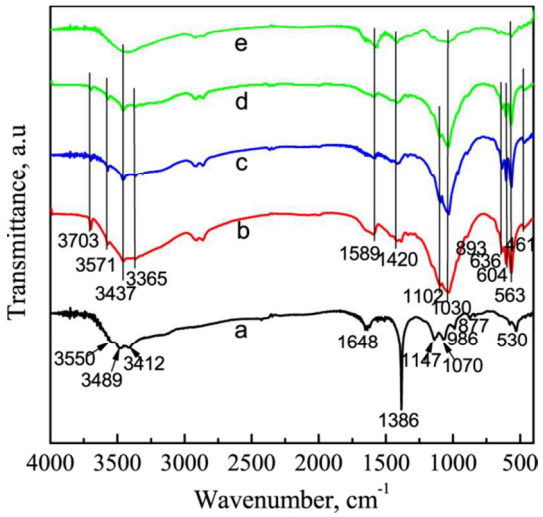

Figure 5 (a) FTIR spectrum of BCCs with the Ca/P ratio of 1.67; FTIR spectra of the HACs converted from the BCCs after hydrothermal reaction at 120°C for different time: (b) 2 h; (c) 1 day; (d) 3 days; (e) FTIR spectrum of chitosan.

Chitosan, a random copolymer of N-acetyl-D-glucosamine and D-glucosamine, is the partially de-acetylated derivative of chitin. The functional groups of chitosan are detected by FTIR spectrum in Figure 5e. The band at 1589 cm^{-1} is assigned to the N-H bending vibration overlapping the amide II vibration. C-N stretching vibration occurs at around 1030 cm^{-1} and overlaps the vibration from the carbohydrate ring. The broad band at around 3437 cm^{-1} is corresponding to the stretching vibration of N-H and OH groups. The $-CH_2$ bending vibration occurs at 1420 cm^{-1}.[19] During the conversion of BCCs into HACs under the hydrothermal conditions, the chitosan in the BCCs is remained. The characteristic bands of chitosan at 1420 cm^{-1} and 1589 cm^{-1} are observed in the HACs (Figure 5). However, its characteristic bands at 1030 and 3437 cm^{-1} are overlapped by those of HA crystals (Figure 5). In order to determine the percentage of chitosan in the HACs, TG and DTA analyses were carried out. The weight loss of 4% between 30°C and 180°C is due to the loss of physically adsorbed water on the HACs (Figure 6).[20] The weight loss of 28.5% at the temperature range 180-550°C belongs to the decomposition of chitosan, suggesting that the content of chitosan is about 28.5% of the total in HACs.[20] The above results can be confirmed by the DTA pattern of HACs (Figure 6). The endothermic peak at around 88°C and exothermic peak at around 278°C are associated with evaporation of adsorbed water and thermal decomposition of chitosan, respectively.

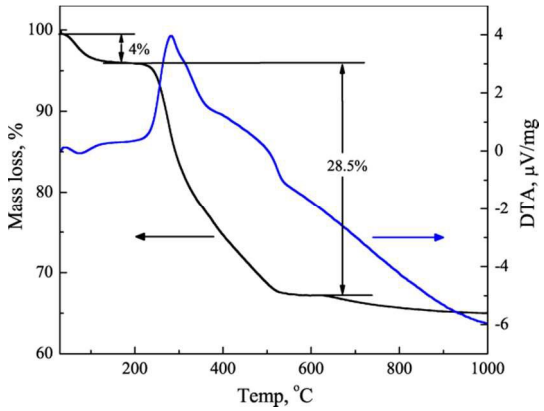

Figure 6 TG and DTA curves of the MHACs converted from the MBGCs with the Ca/P ratio of 1.67 after hydrothermal reaction for 24 h.

In addition, the effects of Ca/P ratios in the BCCs on the morphologies and structures of HACs are discussed in the following text. As we know, stoichiometric HA has a hexagonal crystal structure with the $P6_3/m$ space group, and its Ca/P ratio is 1.67. The original Ca/P ratio in the BCCs had great effect on the morphologies of the HACs, as shown in Figures 1 and 7. If the Ca/P ratio in the BCCs is 1.0, the obtained HA nanoplates have the thicknesses of ~40 nm and widths (or lengths) of 1~2 μm. With increasing the Ca/P ratio from 1.0 to 2.0, the thicknesses and widths (or lengths) decrease gradually. Notably, if the Ca/P ratio in the BCCs is 2.0, the HA nanoplates curl up, and they have the smallest particle size with thicknesses of ~8 nm and widths (or lengths) of 100~300 nm among the three samples with Ca/P ratios of 1.0, 1.67 and 2.0.

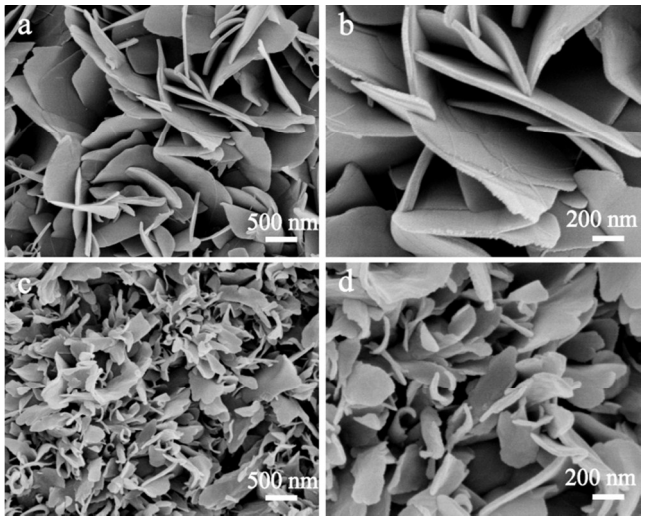

Figure 7 SEM images of HACs converted from CCPs with the different Ca/P ratio after hydrothermal reaction for 24 h: (a,b) 1.0; (c,d) 2.0.

Figure 8 shows the XRD patterns of the HACs converted from the BCCs with the different Ca/P ratios after hydrothermal reaction at 120°C for 24 h. Lin et al. have demonstrated that calcium phosphate phases include HA with a Ca/P molar ratio of 1.67, OCP with a Ca/P molar ratio of 1.33, α- or β-

tricalcium phosphate (α- or β-TCP, $Ca_3(PO_4)_2$) with a Ca/P molar ratio of 1.5 and DCPD with a Ca/P molar ratio of 1.0.[21] Although the BCCs with different Ca/P ratios of 1.0-2.0 are used as precursors, all the obtained products are HA phase. No other calcium phosphate phases are detected in the XRD pattern (Figure 8), suggesting that the original Ca/P ratios have no effect on the phases of products. Moreover, the functional groups of the HACs converted from the BCCs with the different Ca/P ratios are demonstrated by FTIR spectra. Both the characteristic bands due to HA and chitosan are observed for the three samples (Figure 9). Therefore, we can conclude that the original Ca/P ratios in the BCCs have no great effects on the functional groups and phases of the final products.

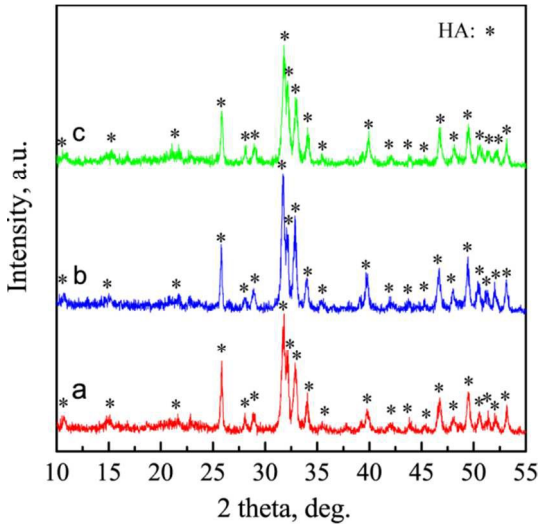

Figure 8 (a) XRD patterns of the HACs converted from the BCCs with the different Ca/P ratio after hydrothermal reaction at 120°C for 24 h: (a) 1.0; (b) 1.67; (c) 2.0.

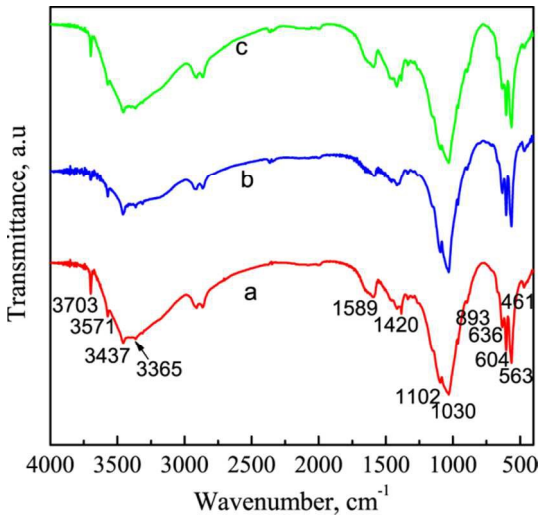

Figure 9 FTIR spectra of the HACs converted from the BCCs with the different Ca/P ratio after hydrothermal reaction at 120°C for 24 h: (a) 1.0; (b) 1.67; (c) 2.0.

3.4 Formation mechanism of HACs

Carbonated calcium-deficient apatite is the main inorganic constituent of human hard tissues including bones and teeth. Depending on the type of hard tissues, apatite crystals possess different orientations. Generally, in the long bones, the *c*-axes of apatite crystals are parallel to the extending collagen fibers, resulting in exposure of their *a*,*b*-planes on the bone surfaces.[6] On the other hand, in the dental enamel, the *a*(*b*)-axes of apatite crystals are perpendicular to the teeth surfaces. The anisotropic characteristics of *a*,*b*-plane and *c*-plane for HA crystals have great effects on bioactivity, biodegradability, and biocompatibility.[7] HACs with oriented nanorod arrays along the *c*-axis have been fabricated by electrochemical deposition, and ZnO-seeded method and hydrothermal method.[7] However, the plate-like HACs with preferred *c*-plane (*a*,*b*-axis) orientations have rarely been reported because HA single crystals grow easily along the *c*-axis. Recently, the biomineralization mechanism of bone minerals has been reported by several research groups.[18] The apatite crystals in natural bones do not initially nucleate within the hole zones, but rather a liquid-phase amorphous precursor is drawn into the collagen fibers via capillary action, and the precursor crystallizes to form apatite crystals by using metastable crystalline phases such as OCP and DCPD as transitory precursors.[22] Based on the formation process of the apatite crystals in natural bones, we fabricated HACs with oriented nanoplate arrays by using BCCs as precursors, as shown in Figure 10.

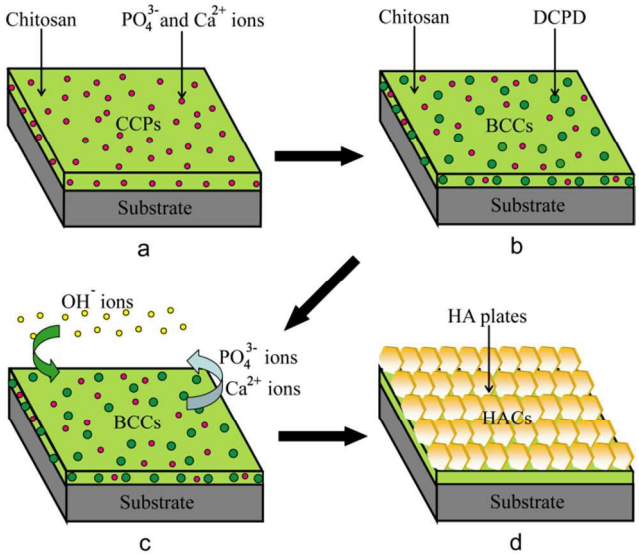

Figure 10 Illustration of the fabrication strategy of HACs with oriented nanoplate arrays: (a) deposition of precursor coatings (CCPs) containing chitosan, Ca^{2+} and PO_4^{3-} ions on Ti6Al4V substrates; (b) formation of BCCs after drying CCPs at room temperature for 48 h; (c) immersion of BCCs in a NaOH solution; (d) fabrication of HACs with oriented nanoplate arrays.

First, the precursors including chitosan, Ca^{2+} ions and PO_4^{3-} ions were prepared by the addition of $Ca(NO_3)_2{\cdot}4H_2O$ and $NaH_2PO_4{\cdot}2H_2O$ into chitosan/acetic acid solutions. Since $Ca(NO_3)_2$ and NaH_2PO_4 could be dissolved in acetic acid solutions, no calcium phosphate phases existed in the sol-like precursors. Second, the sol-like precursors including chitosan, Ca^{2+} ions and PO_4^{3-} ions deposited on Ti6Al4V substrates by dip-coating method (Figure 10a). After drying at room temperature for 48 h, DCPD crystals were formed *in situ* on the coatings

(BCCs) due to the volatilization of acetic acid (Figure 10b). The main inorganic phase of BCCs is DCPD, as confirmed by XRD pattern (Figure 4a).These DCPD particles are covered with chitosan, so the BCCs have smooth surfaces (Figure 1a). Finally, after hydrothermal treatment with a NaOH solution, the BCCs were converted into the HACs. Notably, the chitosan remains on the coatings rather than diffuse into the solution (Figures 5 and 6). The main reason may be attributed to the unique structure of chitosan. Chitosan is a random copolymer of N-acetyl-D-glucosamine and D-glucosamine.[20] The presence of amino groups makes chitosan exist in a soluble or solid state, which depends on the pH value of environments. The chitosan with solid state is not easily dissolved into the NaOH solution because of the stereoregularity and molecular hydrogen bonding among chitosan molecules. Since the logarithmic solubility product of DCPD (pK_{sp}=6.622) is lower than that of HA (pK_{sp}=58.6), HA is more stable in solutions than DCPD.[10b] Under hydrothermal conditions, the BCCs can be converted into the HACs. The morphology of the BCCs is different from that of the HACs (Figure 1), suggesting that the conversion mechanism is a dissolution-precipitation reaction.

After soaking the BCCs in a NaOH solution, the Ca^{2+} and PO_4^{3-} ions are dissolved from the DCPD in the coatings, and enter into the solution. The concentrations of Ca^{2+} and PO_4^{3-} ions exhibit gradient distributions and decrease gradually from the coatings to solution.

$$CaHPO_4 \cdot 2H_2O + OH^- \rightarrow Ca^{2+} + PO_4^{3-} + 3H_2O \quad (1)$$

The released Ca^{2+} and PO_4^{3-} ions may react with the OH^- ions in the NaOH solution to produce plate-like HA particles as the ionic activity product exceeds the thermodynamic solubility product.

$$10Ca^{2+} + 6PO_4^{3-} + 2OH^- \rightarrow Ca_{10}(PO_4)_6(OH)_2 \quad (2)$$

After soaking the BCCs in a NaOH solution, the Ca^{2+} and PO_4^{3-} ions are released from the coatings because of the dissolution reaction of DCPD (Eq. 1). The HA nanoplates tend to deposit on the coating surfaces rather than in the solution because of the following reasons: first, the concentrations of Ca^{2+} and PO_4^{3-} ions on the coating surfaces are higher than in the solution; secondly, the functional groups such as –OH and -NH_2 in the coatings may serve as active sites to promote the deposition of HA crystals.

The reaction time has great effect on the morphologies of the HACs. After the hydrothermal reaction for 2 h, the HA nanoplates with widths (or lengths) of ~100 nm are observed in SEM image (Figures 3a and b). These nanoplates are perpendicular to on the surface of the HACs. With increasing the reaction time from 2 h to 24 h, the widths (or lengths) of HA nanocrystals grows gradually (Figures 1b and 3a). Unfortunately, if the reaction time prolongs upon 3 days, the obtained HA plates on the HACs exhibit an uneven particle size ranging from 100 nm to 800 nm. Moreover, the HA plates begin to curl up. The obvious changes of morphologies with increasing reaction time can be demonstrated by the evolution process of HA crystals. The formation process of the HA particles on the coatings is divided into two stages, including nucleation and growth.[23] The velocity of nucleation is proportional to the relative supersaturation, while that of growth is proportional to the absolute supersaturation.[24] Since the solubility of HA is small (pK_{sp}=58.6), the absolute saturation has a greater effect on the velocity of nucleation than that of growth. If the absolute saturation is large, the velocity of nucleation is greater than that of growth, giving rise to forming lots of nanocrystals; on the contrary, the as-formed nuclei begin to grow.[24] The relative supersaturation and absolute supersaturation for the HA crystals are mainly determined by the concentrations of the Ca^{2+} and PO_4^{3-} ions, which are derived from BCCs. At the initial stage, a number of Ca^{2+} and PO_4^{3-} ions are released from BCCs. The great concentrations of reactants increase the absolute saturation, resulting in the greater velocity of nuclei formation than their growth. Lots of HA nanocrystals are formed on the surface of BCCs after treatment with the NaOH solution for 2 h (Figure 3a). Upon increasing the immersion time, the concentrations of the Ca^{2+} and PO_4^{3-} ions decrease because they are consumed in the initial stages. Under the low absolute saturation, the HA nanoplates tend to grow. The widths (or lengths) of HA nanoplates increased from ~100 nm to ~300 nm with prolonging the reaction time from 2 h to 24 h (Figures 1b and 3a). If the hydrothermal reaction increases up to 3 days, some HA nanoplates become bigger and the others become smaller than those obtained after reaction time of 24 h. Moreover, the numbers of HA plates on the coating surfaces decrease, and they are 231.0, 77.1 and 19.4 per square micron when the reaction times are 2 h, 24 h and 3 days, respectively. This phenomenon can be demonstrated by Ostwald ripening rule.[25] Larger HA particles may grow further at the expense of smaller particles in order to reach a more thermodynamically stable state wherein the surface to area ratio is minimized.

In our previous work, we have developed the HACs with oriented nanorod arrays by using bioglass coatings (BGCs) as precursors in SBF.[7e] Under the hydrothermal conditions, the elongated HA nanorods with *c*-axis orientation deposit on the surfaces via a dissolution-precipitation reaction. With increasing the reaction time from 2 h to 2 days, some HA nanorods are transformed into blocky particles and no plate-like HA particles are obtained.[7e] Interestingly, the HA crystals in the HACs exhibit plate-like shape rather than rod-like shape. Zhuang et al. have reported that HA crystals possess preferred *c*-plane and *a*(*b*)-plane orientations with the different atomic arrangement.[6] The *a*(*b*)-plane is rich in calcium ions, while the *c*-plane is rich in phosphate and hydroxide ions.[6] In the present work, the NaOH solution is used as a reaction solvent to convert the HACs from the BCCs. The high concentration of OH^- ions tends to promote the formation of plate-like HA crystals. In addition, the Ca/P ratios of the CCPs have great effect on the morphologies of HA crystals on the HACs. Under the same amount of Ca^{2+} ions in the BCCs, the widths of HA nanoplates with *c*-plane orientation increase with increasing the amount of PO_4^{3-} ions. If the Ca/P ratio of the BCCs is 2.0, the length (or width) of the HA crystals is 100~300 nm. When the Ca/P ratio decreases to 1.0, the length (or width) of HA plates increases upon 1~2 μm (Figure 7). In contrast, the HA nanorods with *a*(*b*)-plane orientation deposit on the surfaces of the BGCs, since the release amounts of PO_4^{3-} and Ca^{2+} ions are related to their original percentages in the BGCs.

3.5 In vitro bioactivity of HACs

Previous reports have indicated that *in vitro* bioactivity of is assessed by soaking biomaterials in SBF and monitoring the

formation of apatite on the surfaces.[26] The HACs with oriented nanoplate arrays have been prepared from the BCCs after hydrothermal treatment with the NaOH solution for 24 h (Figures 1, 4 and 5). Interestingly, abundantly apatite deposits on the surfaces of HACs after soaking in SBF at 37°C for 3 days (Figure 11a). In addition, gel-like materials are detected in the SEM image, which are ascribed to amorphous calcium phosphate (ACP). Yan et al. have found the formation of ACP on ordered mesoporous bioactive glass after soaking in SBF, too.[27] The ACP as precursor can be converted to apatite both *in vitro* and *in vivo* with increasing the incubation time.[27] Although all HA particles on the HACs before and after soaking in SBF exhibit plate-like shapes, they have different morphologies and chemical components. The high magnification SEM images indicates that the thickness of HA nanoplates formed in SBF is about 40 nm, while those on the HACs is only about 10 nm (Figures 1c and 11a). The EDS spectrum in Figure 11b shows the chemical elements including Ca, P, O, C, Na, Al and Ti, which are mainly derived from the apatite, chitosan and Ti6Al4V substrates.

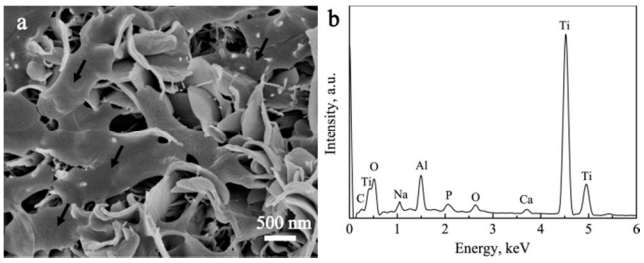

Figure 11 (a) SEM images and (b) corresponding EDS spectrum of HACs after soaking in SBF at 37°C for 3 days. The arrows in (a) show the gel-like ACP.

After soaking the HACs in SBF at 37°C for different days, Ca and P concentrations were determined by ICP-OES, as shown in Figure 12. The concentration changes for Ca and P follow a similar trend. Both the Ca and P concentrations in SBF decrease obviously in the first 5 days, and then reach the equilibrium with increasing further the immersion time. The immersion time, during which Ca and P concentrations reach a stable value, may be used as one of the criteria to evaluate the *in vitro* bioactivity of biocoatings. For HACs, the time that the Ca and P concentrations reach equilibrium is only 5 days, suggesting that the HACs have good *in vitro* bioactivity.

Taken together, both SEM images and ICP-OES investigations reveal that the HACs with oriented nanoplate arrays can promote the formation of apatite on their surfaces (Figures 11 and 12). Kokubo et al. have demonstrated that the essential requirement for a material to bond to living bone is the formation of apatite on its surface when implanted in the living body.[28] Therefore, we can infer that the HACs with oriented nanoplate arrays have potential for implants of human hard tissues. The rapid formation of on the surfaces of the HACs may be attributed to their porous structure, chemical component and crystallographic orientation. Firstly, the nonuniform pores with a pore size of about 20-200 nm among the HA nanoplates help to accelerate the kinetic deposition process of apatite (Figure 1c). The pores in the HACs increase the surface area of the coatings, so many Ca^{2+} and PO_4^{3-} ions are attracted to their surfaces and enter into the inner layer of coatings by using the pores as ion-transfer channels. As the local ion activity product exceeds its thermodynamic solubility product, the apatite deposits on the surfaces of HACs. Secondly, the HA nanoplates on the HACs exhibit preferred *c*-plane orientation, which is rich in phosphate and hydroxide ions. The rich phosphate and hydroxide ions tend to adsorb the Ca^{2+} ions in SBF via electrostatic interactions. The increase of local supersaturation around the HA nanoplates improves the formation of apatite on the HACs. Thirdly, the $-NH_2$ groups in the chitosan can serve as the active sites, which can attach the Ca^{2+} ions and promote the nucleation of apatite.

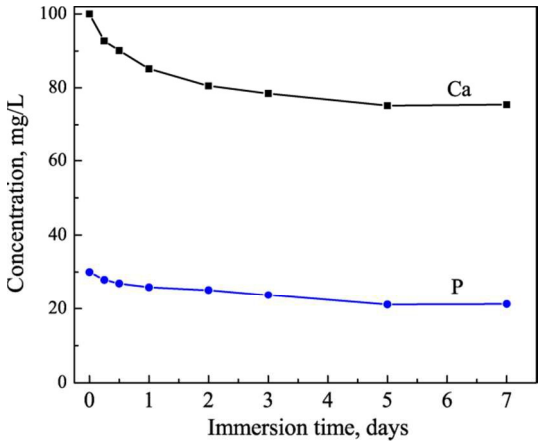

Figure 12 Ca, P concentrations in SBF as a function of immersion time after soaking HACs at 37°C.

3.6 Cell performances of hBMSCs on HACs

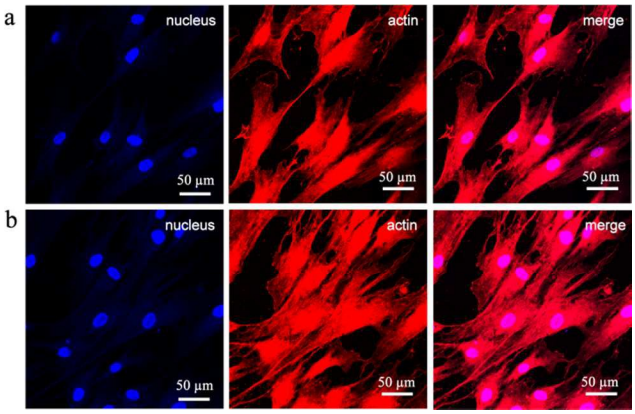

Figure 13 LSCM images of hBMSCs cultured on the different samples: (a) Ti6Al4V, (b) HACs. The cells were stained with blue and red fluorescence, the actin filaments were stained as red fluorescent light and the nucleation were stained as blue fluorescent light.

The cytocompatibility of HACs was investigated by using hBMSCs as cell models and Ti6Al4V substrates as control samples. Figure 13 shows the LSCM images of the hBMSCs cultured on HACs and Ti6Al4V for 24 h. An actin cytoskeleton and focal adhesion staining kit is used to map the orientation of actin filaments with TRITC phalloidin and labeling nuclei with DAPI. The long red bundles of stress fibers composed of actin filaments and good cell-cell contact with one another demonstrate the good cell cytoskeleton morphology of the hBMSCs on the HACs and Ti6Al4V. Notably, as compared with the Ti6Al4V, the hBMSCs cultured on the HACs exhibit rearranged cytoskeleton with better-developed stress actin fibers (Figure 13), suggesting

that the HACs possess better cell adhesion and spreading than Ti6Al4V. CCK-8 assay is a quick and effective method for testing mitochondrial impairment and correlates quite well with cell proliferation.[29] Figure 14 shows the CCK-8 results of the hBMSCs cultured on HACs and Ti6Al4V at the different days. With increasing the culture time, the number of viable cells increases gradually. For both groups, the cell number of the hBMSCs at day 7 is more than three times that of day 1. Both the LSCM images and CCK-8 assay results reveal that the Ti6Al4V and HACs exhibit good cytocompatibility (Figures 13 and 14), which can promote the cell adhesion, spreading and proliferation. Interestingly, the HACs possess better cell biological properties such as the adhesion, spreading and proliferation than the Ti6Al4V substrates.

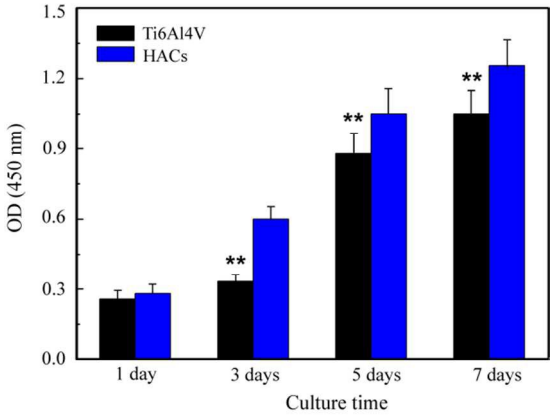

Figure 14 CCK-8 assay results of hBMSCs cultured on the Ti6Al4V and HACs at different days. The data are represent as the means±standard deviation; n=3 (** p<0.01).

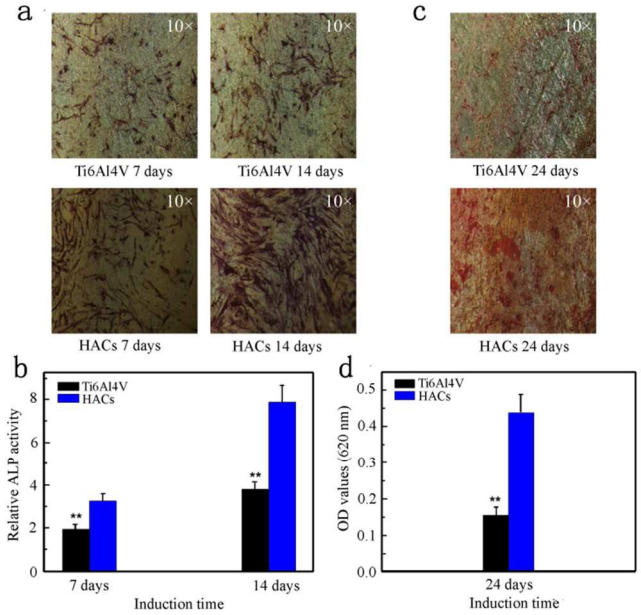

Figure 15 (a) ALP staining and (b) ALP activity of hBMSCs grown on the Ti6Al4V and HACs after 7 and 14 days. (c) Alizarin red staining and (d) corresponding quantitative analysis results of hBMSCs grown on the Ti6Al4V and HACs after 24 days (** p<0.01).

To investigate the osteogenic differentiation of hBMSCs on different substrates, ALP activity and mineralization were measured in vitro. In the process of hBMSCs osteogenesis, ALP is an early marker for osteoblast differentiation, which involves the degradation of inorganic pyrophosphate to provide sufficient local concentrations of phosphate for mineralization.[30] Figure 15a shows the typical ALP staining results of hBMSCs in the osteogenic medium after 7 and 14 days. The ALP staining intensity of the hBMSCs on the HACs is stronger than that on the Ti6Al4V substrates. Figure 15b shows the relative ALP activity results for the HACs and Ti6Al4V at 7 and 14 days. Both samples exhibit a similar time-dependent increase in ALP activity from 7 days to 14 days. Interestingly, the cells on the HACs have a higher ALP activity than those on Ti6Al4V (p<0.01). The results of ALP staining and ALP activity suggest that the osteogenic differentiation of the hBMSCs is enhanced on the HACs as compared with the Ti6Al4V substrates. In addition, the extracellular matrix mineralization was assessed by alizarin red staining, as shown in Figures 15c and d. More calcium nodules are formed on the HACs than on the Ti6Al4V after culturing for 24 days (Figure 15c). Quantitative analysis of the alizarin red staining in Figure 15d indicates that the HACs exhibit clearly higher mineralization than the Ti6Al4V (p<0.01), which is consistent with ALP activity results (Figures 15a and b).

The better adhesion, spreading, proliferation and osteogenic differentiation of the hBMSCs on the HACs than on the Ti6Al4V may be attributed to the presence of HA nanoplates with preferred c-plane orientations. Firstly, the HACs have pores among the HA nanoplates, which increase contacting areas and roughness. Large contacting areas are preferable for cell attachment, spreading and proliferation.[31] At the same time, cell adhesion, proliferation and detachment strength are sensitive to surface roughness. The surface roughness of the coatings can improve the short- and longer-term response of cells.[32] Costa et al. have reported that increased levels of surface roughness and complexity could enhance collagen type I and alkaline phosphatase expression, consistent with accelerated differentiation.[33] Secondly, chitosan originated from hard shell of insects and crustaceans has good cytocompatibility, biodegradability and bioactivity.[34] The presence of chitosan in the HACs may improve the adhesion, proliferation and osteogenic differentiation of hBMSCs.[35] Amir et al. have reported that Chitosan can significantly enhance RUNX2 and ALP mRNA, and tend to increase the release of ALP hydrolytic enzyme activity into the medium during the first week.[36] Finally, the HA c-plane orientation on the HACs have great effect on cell performances. The a(b)-plane of HA crystals is rich in calcium ions with positive charges, while the c-plane is rich in phosphate and hydroxide ions with negative charges.[6] Since the HA crystals on the HACs exhibit c-plane orientation, more phosphate and hydroxide ions exist on the surface, resulting in negative surfaces, great wettability and high energy surfaces. Generally, a high-energy surface will improve cell attachment, spreading and osteogenic differentiation.[37] In contrast, Zhuang et al. have reported that the adhesion efficiency of MC3T3-E1 cells decrease with increasing initial a(b)-plane orientation degree.[6a] Therefore, the hBMSCs on the HACs with oriented nanoplate arrays have good cell morphology, cytoskeletal organization, cell attachment, spreading and proliferation.

4. Conclusions

HACs with oriented nanoplate arrays are converted from BCCs by hydrothermal treatment with alkaline solutions. After soaking the BCCs in a NaOH solution, the Ca^{2+} and PO_4^{3-} ions are released from the BCCs, and react with OH^- ions to form HA nanoplates under hydrothermal conditions. These HA nanoplates with a preferential *c*-plane orientation are perpendicular to the coating surfaces. Hydrothermal reaction time and Ca/P ratio of BCCs have great effect on the morphologies of HA nanoplates. With increasing the reaction time from 3 h to 3 days or decreasing the Ca/P ratio from 2.0 to1.0, the widths (or lengths) of HA nanoplates increase gradually. The HACs with oriented nanoplate arrays have good *in vitro* bioactivity, which can promote the formation of apatite on the surfaces. Moreover, the hBMSCs on the HACs have good cell adhesion, spreading and proliferation because of the similar chemical component, plate-like shape and crystallographic orientation to bone minerals. Therefore, the HACs with oriented nanoplate arrays have great potential for bone implants.

Acknowledgements

This research was supported by Key Disciplines of Shanghai Municipal Education Commission (No. J50206), Natural Science Foundation of China (Nos. 51002095, 51372152 and 30973038), Science and Technology Commission of Shanghai Municipality (No. 12JC1405600), Program of Shanghai Normal University (Nos. DZL124, DCL201303), Innovation Foundation of Shanghai Education Committee (No. 14ZZ124), and State Key Laboratory for Modification of Chemical Fibers and Polymer Materials, Dong Hua University (No. LK1206).

Notes and references

1 a) Y. Chen, B. Bai, S. Zhang, J. Ye, H. Zhai, Y. Chen, L. Zhang and Y. Zeng, *J. Biomed. Mater. Res. A,* 2014, **102A**, 1294; b) J. S. Harris, T. B. Bemenderfer, A. R. Wessel and M. A. Kacena, *Bone*, 2013, **55**, 241; c) S. Samavedi, A. R. Whittington and A. S. Goldstein, *Acta Biomater.,* 2013, **9**, 8037; d) X. Y. Yuan, B. S. Zhu, G. S. Tong, Y. Su and X. Y. Zhu, *J. Mater. Chem. B,* 2013, **1**, 6551; e) X. M. Zhang, C. T. Wu, J. Chang and J. Sun, *J. Mater. Chem. B,* 2014, **2**, 885.

2 a) S. R. Paital and N. B. Dahotre, *Mater. Sci. Eng. R,* 2009, **66**, 1-70. b) A. Krzakala, A. Kazek-Kesik and W. Simka, *RSC Adv., 2013*, **3**, 19725; c) R. Ion, D. M. Gordin, V. Mitran, P. Osiceanu, S. Dinescu, T. Gloriant and A. Cimpean, *Mater. Sci. Eng. C,* 2014, **35**, 411; d) M. Niinomi, M. Nakai and J. Hieda, *Acta Biomater.,* 2012, **8**, 3888. e) R . Huang, Y. Han and S. M. Lu, *J. Mater. Chem. B*, 2014, **2**, 4531.

3 a) C. X. Yue, R. Kuijer, H. J. Kaper, H. C. van der Mei and H. J. Busscher, *Biomaterials,* 2014, **35**, 2580; b) S. F. M. van Dongen, P. Maiuri, E. Marie, C. Tribet and M. Piel, *Adv. Mater.,* 2013, **25**, 1687; c) N. J. Shah, J. Hong, M. N. Hyder and P. T. Hammond, *Adv. Mater.*, 2012, 24, 1445.

4 a) H. X. Zhao, W. J. Dong, Y. Y. Zheng, A. P. Liu, J. M. Yao, C. R. Li, W. H. Tang, B. Y. Chen, G. Wang and Z. Shi, *Biomaterials*, 2011, **32**, 5837; b) R. Rojaee, M. Fathi and K. Raeissi, *Mater. Sci. Eng. C,* 2013, **33**, 3817; c) S. Mahmoodi, L. Sorkhi, M. Farrokhi-Rad and T. Shahrabi, *Surf. Coat. Technol.,* 2013, **216**, 106; d) A. Cattini, D. Bellucci, A. Sola, L. Pawlowski, V. Cannillo, *J. Biomed. Mater. Res. B Appl. Biomater.,* 2014, **102**, 551.

5 a) N. Almora-Barrios, K. F. Austen and N. H. De Leeuw, *Langmuir,* 2009, **25**, 5018; b) J. Liu, X. Wang, Q. Jin, T. Jin, S. Chang, Z. Zhang, A. Czajka-Jakubowska, W. V. Giannobile, J. E. Nör and B. H. Clarkson, *Biomaterials,* 2012, **33**, 5036; c) J. Liu, T. Jin, S. Chang, A. Czajka-Jakubowska, Z. Zhang, J. E. Nör and B. H. Clarkson, *Tissue Eng. Part A,* 2010, **16**, 2977; d) X. L. Dong, H. L. Zhou, T. Wu and Q. Wang, *J. Phys. Chem. B,* 2008, **112**, 4751; e) J. Liu, T. C. Jin, S. Chang, A. Czajka-Jakubowska and B. H. Clarkson, *J. Biomed. Mater. Res. A,* 2011, **96A**, 528-534; f) X. Liu, K. Lin, R. Qian, L. Chen, S. Zhuo and J. Chang, *Chem. Eur. J.,* 2012, **18**, 5519.

6 a) Z. Zhuang, T. J. Fujimi, M. Nakamura, T. Konishi, H. Yoshimura and M. Aizawa, *Acta Biomater*., 2013, **9**, 6732; b) Z. Zhuang and M. Aizawa, *J. Mater. Sci.: Mater. Med.,* 2013, **24**, 1211; c) Z. Zhuang, H. Yoshimura, M. Aizawa, *Mater. Sci. Eng. C*, 2013, **33**, 2534.

7 a) G. Wang, Z. Lu, X. Zhao, A. Kondyurin and H. Zreiqat, *J. Mater. Chem. B,* 2013, **1**, 2455; b) E. A. dos Santos, M. S. Moldovan, L. Jacomine, M. Mateescu, J. Werckmann, K. Anselme, P. Mille and H. Pelletier, *Mater. Sci. Eng. B,* 2010, **169**, 138; c) Z. Lu, H. Xu, M. Xin, K. Li and H. Wang, *J. Phys.Chem. C,* 2010, **114**, 820; d) W. Chen, T. Long, Y. J. Guo, Z. A. Zhu and Y. P. Guo, *J. Mater. Chem. B*, 2014, **2**, 1653-1660; e) W. Chen, T. Long, Y. J. Guo, Z. A. Zhu and Y. P. Guo, *RSC Adv*., 2014, **4**, 185.

8 a) M. J. Olszta, X. Cheng, S. S. Jee, R.kumar, Y. Y. Kim, M. J. Kaufman, E. P. Douglas and L. B. Gower, *Mater. Sci. Eng. R,* 2007, **58**, 77; b) T. Hassenkam, G. E. Fantner, J. A. Cutroni, J. C. Weaver, D. E. Morse and P. K. Hansma, *Bone* 2004, **35**, 4; c) M. Tzaphlidou, *J. Biol. Phys*. 2008, **34**, 39-49.

9 a) J. Ryu, S. H. Ku, H. Lee and C. B. Park, *Adv. Func. Mater.,* 2010, **20**, 2132; b) Y. Guo, Y. Zhou and D. Jia, *Acta Biomater.,* 2008, **4**, 334; c) Y. Guo and Y. Zhou, *J. Biomed. Mater. Res. A*, 2008, 86A, 510; d) F. Thammarakcharoen, W. Suvannapruk and J. Suwanprateeb, J. *Nanosci. Nanotechnol.,* 2014, **14**, 7614.

10 a) A. Oyane, H. M. Kim, T. Furuya, T. Kokubo, T. Miyazaki, T. Nakamura, *J. Biomed. Mater. Res. A,* 2003, **65A**, 188; b) X. Lu and Y. Leng. *Biomaterials,* 2005, **26**,1097.

11 H. Tan, Z. Peng, Q. Li, X. Xu, S. Guo and T. Tang, *Biomaterials,* 2012, **33**, 365.

12 T. Long, Y. P. Guo, S. Tang, Y. J. Guo and Z. A. Zhu, *RSC Adv.,* 2014, **4**, 11816; Dongwoo Khang, J. Choi, Y.-M. Im, Y.-J. Kim, J.-H. Jang, S. S. Kang, T.-H. Nam, J. Song and J.-W. Park, *Biomaterials*, 2012, **33**, 5997

13 Q. Fan, T. Tang, X. Zhang and K. Dai, *J. Cell. Mol. Med.,* 2009, **13**, 2489.

14 L. Tortet, J. R. Gavarri and G. Nihoul, *J. Solid State Chem.,* 1997, **132**, 6.

15 C. B. Baddiel, E. E. Berry, *Spectrochim. Acta*, 1966, **22**, 1407.

16 D. Walsh, T. Furuzono and J. Tanaka, *Biomaterials,* 2001, **22**, 1205.

17 a) A. Badri, C. Binet J.-C. Lavalley, *J. Chem. Soc., Faraday Trans.* 1996, **92**, 4669; b) R.N. Panda, M.F. Hsieh, R.J. Chung, T.S. Chin, *J. Phys. Chem. Solids*, 2003, **64**, 193.

18 F. Ye, H. Guo, H. Zhang, X. He, *Acta Biomater.,* 2010, **6**, 2212.

19 a) G. Lawrie, I. Keen, B. Drew, L. Rintoul, P. Fredericks and L. Grondahl, *Biomacromolecules*, 2007, **8**, 2533; b) B. Li, Y. Wang, D. Jia, Y. Zhou and W. Cai, *Biomed. Mater.,* 2009, **4**, 015011.

20 a) J. Chen, K. Nan, S. Yin, Y. Wang, T. Wu, Q. Zhang, *Colloid. Surf B,* 2010, **81**, 640; b) P. Venkatesan, N. Puvvada, R. Dash, B. N. Prashanth Kumar, D. Sarkar, B. Azab, A. Pathak, S. C. Kundu, P. B. Fisher and M. Mandal, *Biomaterials*, 2011, **32**, 3794.

21 K. Lin, C. Wu and J. Chang, *Acta Biomater.,* 2014, **10**, 4071.

22 a) M. J. Olszta, X. Cheng, S. S. Jee, R.kumar, Y. Y. Kim, M. J. Kaufman, E. P. Douglas and L. B. Gower, *Mater. Sci. Eng. R,* 2007, **58**, 77; b) F. Nudelman, K. Pieterse, A. George, P. H. H. Bomans, H. Friedrich, L. J. Brylka, P. A. J. Hilbers, G. de With and N. A. J. M. Sommerdijk, *Nat. Mater.,* 2010, **9**, 1004; c) W. Traub, T. Arad and S. Weiner, *Proc. Natl Acad. Sci. USA,* 1989, **86**, 9822.

23 Y. P. Guo, Y. Zhou, D. C. Jia and Q. C. Meng, *ACTA Biomater.,* 2008, **4**, 923.

24 a) H. B. Weiser and A. P. Bloxsom, *J. Phys. Chem.,* 1924, **28**, 26; b) H. B. Weiser and W. O. Milligan, *J. Phys. Chem.,* 1932, **36**, 1950.

25 J. Nývlt, *Cryst. Res. Technol.,* 1995, **30**, 443.

26 a) T. Kokubo and H. Takadama, *Biomaterials*, 2006, **27**, 2907; b) T. Akazawa, M. Murata, J. Hino, F. Nagano, T. Shigyo, T. Nomura, H. Inano, K. Itabashi, T. Yamagishi, K. Nakamura, T. Takahashi, S. Iida and H. Kashiwazaki, *Appl. Surf. Sci.,* 2012, **262**,51.

27 X. Yan, C. Yu, X. Zhou, J. Tang and D. Zhao, *Angew. Chem. Int. Ed.,* 2004, **43**, 5980.

28 T. Kokubo and H. Takadama, *Biomaterials*, 2006, **27**, 2907

29 a) L. X. Lu, X. F. Zhang, Y. Y. Wang, L. Ortiz, X. Mao, Z. L. Jiang, Z. D. Xiao and N. P. Huang, *ACS Appl. Mater. Inter.,* 2013, **5**, 319; b) M. Li, Y. B. Wang, Q. Liu, Q. H. Li, Y. Cheng, Y. F. Zheng, T. F. Xi and S. C. Wei, *J. Mater. Chem. B,* 2013, **1**, 475.

30 Q. Liu, L. Cen, S. Yin, L. Chen, G. Liu, J. Chang and L. Cui, *Biomaterials*, 2008, **29**, 4792.

31 a) Y. Hong, H. Fan, B. Li, B. Guo, M. Liu and X. Zhang, *Mater. Sci. Eng. R*, 2010, **70**, 225; b) X. Li, C.A. Blitterswijk, Q. Feng, F. Cui and F. Watari, *Biomaterials*, 2008, **29**, 3306.

32 a) D. D. Deligianni, N. D. Katsala, P. G. Koutsoukos and Y. F. Missirlis, *Biomaterials*, 2001, **22**, 87; b) M. Lampin, R. Warocquier-Clérout, C. Legris, M. Degrange and M. F. Sigot-Luizard, *J. Biomed. Mater. Res*., 1997, **36**, 99.

33 D. O. Costa, P. D. H. Prowse, T. Chrones, S. M. Sims, D. W. Hamilton, A. S. Rizkalla and S. J. Dixon, *Biomaterials*, 2013, **34**, 7215.

34 a) E. Marin, M. I. Briceno and C. Caballero-George, *Int. J. Nanomed.*, 2013, **8**, 3071; b) W. Graisuwan, O. Wiarachai, C. Ananthanawat, S. Puthong, S. Soogarun, S. Kiatkamjornwong and V. P. Hoven, *J. Colloid Interf. Sci.,* 2012, **376**, 177; c) G. C. Wang, L. Zheng, H. S. Zhao, J. Y. Miao, C. H. Sun, H. Liu, Z. Huang, X. Q. Yu, J. Y. Wang and X. T. Tao, *ACS Appl. Mater. Inter.,* 2011, **3**, 1692.

35 a) H. H. Liu, H. J. Peng, Y. Z. Zhang and H. W. OuYang, *Biomaterials,* 2013, **34**, 4404; b) S. Erakovic, A. Jankovic, D. Veljovic and V. Miskovic-Stankovic, *J. Phys. Chem. B*, 2013, **117**, 1633.

36 L. R. Amir, D. F. Suniarti, S. Utami and B. Abbas, *Cell Tissue Res.,* 2014, 358, 407

37 a) E. S. Thian, Z. Ahmad, J. Huang, M. J. Edirisinghe, S. N. Jayasinghe, D. C. Ireland, R. A Brooks, N. Rushton, W. Bonfield and S. M. Best, Acta biomater., 2010, **6**, 1878; b) K. Anselme, *Biomaterials*, 2000, **21**, 667; c) A. E. Loiselle, L. Wei, M. Faryad, E. M. Paul, G. S. Lewis, J. Gao, A. Lakhtakia and H. J. Donahue, *Tissue Eng. Part A*, 2013, 19, 1704.

[a]*The Education Ministry Key Lab of Resource Chemistry and Shanghai Key Laboratory of Rare Earth Functional Materials, Shanghai Normal University, Shanghai 200234, China. E-mail: ypguo@shnu.edu.cn; Fax: +86-21-64321951; Tel: +86-21-64321951*

[b]*Shanghai Key Laboratory of Orthopedic Implant, Department of Orthopedic Surgery, Shanghai Ninth People's Hospital, Shanghai Jiao Tong University School of Medicine, Shanghai 200011, China. E-mail: zhuzhenan2006@126.com*

[c] *Department of Orthopedics Surgery, Shanghai Sixth People's Hospital, Shanghai Jiaotong University, Shanghai 20200233, China*

† Contributed equally to this work.